RSC Advances

PAPER

View Article Online
View Journal | View Issue

Cite this: *RSC Adv.*, 2026, **16**, 464

Copper nanocluster-mediated degradation of toxic organic dyes: a sustainable approach to water remediation

Aarya, Kavya P., Chanchal N. S., Devika V., Athira Sathyan and Supratik Sen Mojumdar *

Organic pollutants, particularly toxic dyes discharged in large quantities by the textile and food industries, have attracted considerable scientific attention due to their environmental persistence and detrimental effects. Metal nanoclusters (NCs), owing to their redox-active metal cores and tunable surface properties, represent promising candidates for the efficient degradation of such pollutants. In this study, we report an efficient protocol for the degradation of Rhodamine B (RhB) and Methylene Blue (MB) using cysteine-capped copper nanoclusters (Cys-Cu NCs) in the presence of hydrogen peroxide (H_2O_2), without any external stimuli. The degradation, carried out under neutral pH and aqueous conditions, was monitored using UV-visible spectroscopy and showed approximately 97% degradation of both dyes (20 μM) within 90 minutes, accompanied by complete decolourization of the solutions. Characterization of the degradation products using LC-MS, ^{1}H NMR, and ion chromatography confirmed the complete mineralization of the dyes into non-toxic species. Control and free-radical scavenging experiments confirmed that the process proceeds through the synergistic action of Cys-Cu NCs and H_2O_2, primarily involving reactive oxygen species (ROS) such as hydroxyl ($^{\bullet}OH$) and superoxide ($^{\bullet}O_2^-$) radicals, thereby elucidating the underlying degradation mechanism. Comparative studies with other metal nanoclusters highlight that the superior activity of Cys-Cu NCs arises from the intrinsic redox property of copper, which plays a pivotal role in ROS generation and dye degradation. Kinetic analyses revealed that RhB and MB follow distinct degradation pathways. Furthermore, degradation studies performed at varying dye concentrations, larger reaction volumes, and in real water samples demonstrated the robustness and practical applicability of the developed method. Overall, the Cys-Cu NC-mediated degradation offers a sustainable and efficient approach for the remediation of dye-contaminated water.

Received 13th November 2025
Accepted 17th December 2025

DOI: 10.1039/d5ra08780e

rsc.li/rsc-advances

1. Introduction

The rapid pace of industrialization and urbanization over recent decades has had a profound impact on the environment, posing serious threats to ecosystems and human health. Among these, water pollution resulting from the uncontrolled discharge of industrial effluents—such as dyes, pharmaceuticals, toxic metal ions, and acidic compounds—has emerged as a major concern, spurring intensive research efforts toward sustainable remediation strategies.[1–3] Industrial wastewater from sectors such as textiles, food processing, paints, and cosmetics often contains synthetic dyes that are highly toxic, chemically stable, poorly biodegradable, and environmentally persistent. Their release into aquatic systems leads to long-term ecological and health hazards.[3–6] Improper disposal of such dyes not only causes severe water contamination but also imparts intense colouration to water bodies, hindering sunlight penetration, suppressing photosynthetic activity, lowering dissolved oxygen levels, and disrupting the delicate balance of aquatic ecosystems.[6,7] Furthermore, untreated dyes entering the food chain can induce mutagenic, carcinogenic, genotoxic, neurotoxic, teratogenic, and endocrine-disrupting effects, posing grave risks to both humans and other organisms.[4,8]

Several techniques have been developed for treating dyes and organic pollutants, including adsorption,[3,9] ion exchange,[10] chemical oxidation,[11] ultrafiltration,[1,12] vacuum membrane distillation,[13] microwave treatment,[14] coagulation,[15] and photocatalytic degradation.[5,6,16,17] However, many of these methods suffer from low efficiency and/or the generation of harmful secondary pollutants, complicating waste disposal and management.[17–19] Additionally, most conventional approaches are limited by high operational costs, complex procedures, and the need for skilled personnel and advanced technical expertise.[17–19] Among the available strategies, photocatalysis offers distinct advantages owing to its efficiency and environmental sustainability.[5,6,16–18] Under light irradiation and in the presence of a suitable photocatalyst, organic pollutants can be

Department of Chemistry, Indian Institute of Technology Palakkad, Palakkad, Kerala, 678 623, India. E-mail: supratik@iitpkd.ac.in

decomposed into harmless end products.[16,18] Metal nanoparticles exhibit photocatalytic activity when integrated with semiconductor systems such as TiO_2, ZnO, SiO_2, and Nb_2O_5.[19–23] However, in many cases, the photocatalysts themselves exhibit toxicity, posing additional environmental concerns.[17] Alternatively, the advanced oxidation processes (AOPs), which generate reactive oxygen species (ROS), provide an efficient pathway for degrading and mineralizing highly stable organic dyes into carbon dioxide, water, and inorganic ions such as nitrate, sulfate, phosphate *etc.*[17,18,24,25] Environmentally benign redox-active materials capable of generating ROS through AOPs could therefore serve as promising alternatives to conventional toxic photocatalysts for the efficient, irradiation-free degradation of organic dyes.

Metal nanoclusters (NCs), with strong photoluminescence, ultrasmall sub-nanometer core, tunable properties, high stability, and environmental adaptability, generally exhibit low toxicity and therefore could potentially act as promising green redox-active materials for the degradation of toxic dyes.[26–28] Comprising tens to hundreds of metal atoms stabilized by surface ligands such as proteins,[26,29] amino acids,[27,30] DNA,[31] or polymers,[32,33] these ultrasmall entities exhibit remarkable physicochemical properties. Among them, amino acid-capped nanoclusters stand out as versatile materials for a wide range of applications.[27,34–38] Although nanoclusters alone generally lack sufficient capacity for dye degradation and often require coupling with semiconductor systems,[19] a recent study reported that noble metal nanoclusters—specifically silver[39]—can degrade dyes by harnessing their intrinsic photocatalytic properties. However, copper nanoclusters (Cu NCs), despite being more earth-abundant and cost-effective, remain relatively unexplored in this context.

Herein, we aim to degrade the highly toxic dyes Rhodamine B (RhB) and Methylene Blue (MB) using Cu NCs. RhB and MB are widely used synthetic dyes with significant environmental and health concerns. RhB, a photostable, water-soluble xanthene dye, is extensively applied in textiles, food industries, and biological studies such as fluorescence microscopy and cell imaging.[18,40] Its poor biodegradability allows accumulation in aquatic environments, where even 1 mg L^{-1} can harm ecosystems and human health.[24,41] RhB is linked to carcinogenicity, genetic alterations, irritation of skin, eyes, respiratory and gastrointestinal tracts, and reproductive toxicity,[42–44] prompting bans in several countries and classification as a potential carcinogen by the IARC.[45,46] MB, a non-biodegradable dye due to its stable aromatic structure, is toxic and potentially carcinogenic.[47,48] While used medically at low doses (<2 mg kg^{-1})[49,50] for methemoglobinemia, malaria, and as a tracer dye, excessive exposure can cause serotonin toxicity and severe effects on respiratory, renal, cardiovascular, neurological, and reproductive health.[18,51–54] Untreated MB- and RhB-contaminated wastewater also adversely affects aquatic plants and microalgae, inhibiting growth and reducing pigment and protein content.[55]

In this study, a facile cysteine capped copper nanocluster (Cys-Cu NC)-based approach was developed for the rapid and complete degradation of toxic dyes such as RhB and MB, under neutral conditions, without requiring surface modification, any other transition metal doping, or high-intensity irradiation. The choice of Cys-Cu NCs was motivated by their rapid synthesis (within 30 minutes) and relatively high photoluminescence quantum yield compared to other amino acid-capped nanoclusters.[56] Due to their intrinsic redox activity and oxidation propensity, Cu NCs can generate ROS in the presence of hydrogen peroxide (H_2O_2),[25,56] which could potentially enable simple and efficient dye degradation. Upon the addition of Cys-Cu NCs in the presence of the oxidizing agent hydrogen peroxide (H_2O_2), nearly complete degradation (~97%) of both RhB (20 μM; 9.6 mg L^{-1}) and MB (20 μM; 6.4 mg L^{-1}) was achieved within 90 minutes. UV-visible absorption and fluorescence measurements showed a gradual decrease in the characteristic spectral features of the dyes, confirming progressive degradation. The kinetic and mechanistic aspects of the process were systematically investigated, and complete mineralization was verified, indicating the absence of secondary pollutants. Furthermore, the degradation studies conducted in real water samples and at the bulk scale demonstrated the method's robustness and potential for practical wastewater treatment applications. Overall, this study demonstrates a green and sustainable AOP for the complete degradation of organic dyes using Cys-Cu NCs, offering an effective and environmentally benign alternative for wastewater remediation.

2. Materials and methods

2.1. Materials

The L-cysteine (Cys) and L-tryptophan (Trp) used for the synthesis of nanoclusters were purchased from Sisco Research Laboratories Pvt. Ltd (SRL). The corresponding metal precursors of nanoclusters, such as copper nitrate ($Cu(NO_3)_2$), and copper chloride ($CuCl_2$), as well as sodium hydroxide (NaOH), hydrazine monohydrate ($N_2H_4 \cdot H_2O$), hydrochloric acid (HCl) and hydrogen peroxide (H_2O_2) were obtained from Nice Chemicals (NICE). The Rhodamine B (RhB) and Methylene blue (MB) used for the degradation studies were purchased from Tokyo Chemical Industry (TCI). The *tert*-butyl alcohol (TBA) and 2,5-dihydroxy-*p*-benzoquinone (DHBQ) used for the scavenging experiments were procured from Spectrochem Pvt. Ltd and Sigma-Aldrich, respectively. All the reagents were used as received without further purification and all the solutions were prepared using doubly distilled water from the Biopak Polisher Milli-Q water system (CDUFB1001).

2.2. Instrumentation

The UV-visible absorption spectra were recorded from 200 nm to 800 nm with a scan speed of 1200 nm min^{-1} using a Thermo Fisher Scientific UV-visible spectrophotometer (Evolution 201). Photoluminescence (PL) spectra were recorded using a PerkinElmer Fluorescence Spectrometer (FL 6500). The RhB and MB were excited at 553 nm and 665 nm, respectively, with excitation and emission slit widths of 10 nm at a scan speed of 240 nm min^{-1}. X-ray photoelectron spectroscopy (XPS) analysis was performed using a Thermo Scientific NEXSA Surface Analysis system. The end products of the degradation were characterized using a Liquid Chromatograph-Mass Spectrometer (LC-MS; Shimadzu Scientific Instruments, Model: LCMS 8045),

a Proton Nuclear Magnetic Resonance (^{1}H NMR) spectrometer (JEOL, Model: JNM-ECZ500R), and an Ion Chromatograph (Metrohm, Model: 930 IC). The Cys-Cu NC solution was centrifuged using a non-refrigerated centrifuge from Dinesh Scientific (Model no: DS-NRC-473).

2.3. Synthesis of metal nanoclusters

2.3.1. Cys capped copper nanocluster (Cys-Cu NC). Cys-Cu NCs were prepared following a previously reported protocol.[56] Briefly, an aqueous solution of Cys (360 μL of 50 mM (6 mg mL^{-1})) was mixed with $Cu(NO_3)_2$ (90 μL of 100 mM (24 mg mL^{-1})) and 2550 μL of MilliQ water to obtain a final Cys concentration of 6 mM and a $Cu(NO_3)_2$ concentration of 3 mM in a total reaction volume of 3 mL (Cu : Cys molar ratio = 1 : 2). The mixture was stirred at room temperature for 2 minutes. The pH of the mixture was then adjusted to 11 by the dropwise addition of 300 μL of 1 M NaOH, followed by continued stirring for 30 minutes. The resulting solution was centrifuged at 14 000×g for 30 minutes to remove larger particulates. The supernatant containing the Cys-Cu NCs was collected and stored in the dark at 4 °C for further use.

2.3.2. Trp capped copper nanocluster (Trp-Cu NC). Trp-Cu NCs were synthesized following a previously reported procedure.[27] An aqueous solution of Trp (833 μL of 18 mM (3.7 mg mL^{-1})) was mixed with $CuCl_2$ solution (1.5 μL of 100 mM (17 mg mL^{-1})) and 2165.5 μL of MilliQ water to obtain a final concentration of 5 mM tryptophan and 0.05 mM $CuCl_2$ (Trp : Cu molar ratio = 100 : 1) in a total reaction volume of 3 mL. The reaction mixture was then stirred at 40 °C for 30 minutes. The pH of the solution was then adjusted to 12 by adding 100 μL of 1 M NaOH, followed by stirring at room temperature for an additional 30 minutes. Subsequently, 50 μL of 80% hydrazine monohydrate was added, and the reaction mixture was stirred continuously at 40 °C for 8 hours. The resulting Trp-Cu NCs were stored in the dark at 4 °C for further use.

2.4. Degradation of RhB and MB

The degradation of RhB and MB was carried out separately following an identical procedure. Initially, 2 mL of Cys-Cu NC solution was taken, and the pH was adjusted to 7 by adding an appropriate amount of 1 M HCl. Subsequently, 10.2 μL of 30% H_2O_2 was added to achieve a final concentration of 50 mM in the reaction mixture. This was followed by the addition of 26.7 μL of 1.5 mM of the respective dye solution to obtain a final dye concentration of 20 μM. The absorption spectra were immediately recorded using a UV-visible spectrophotometer. RhB and MB exhibited maximum absorbance at 553 nm and 665 nm, respectively. The reaction mixture was then stirred vigorously at 50 °C, and the absorption spectra were recorded at regular time intervals. The dye concentrations at different time points were determined using the Beer–Lambert law:

$$A = \varepsilon c l \quad (1)$$

where A is the absorbance at the absorption maxima (λ_{max}), ε is the molar extinction coefficient (106 000 L mol^{-1} cm^{-1} at 553 nm for RhB[57] and 74 100 L mol^{-1} cm^{-1} at 665 nm for MB[58]) l is the path length and c is the concentration (mol L^{-1}). The degradation efficiency was calculated using the equation:

$$\%\ \text{degradation} = \frac{(C_0 - C_t)}{C_0} \times 100 \quad (2)$$

where C_0 and C_t represent the dye concentrations at time 0 and t, respectively.

2.5. Kinetics of dye degradation

To investigate the degradation kinetics of RhB and MB in the presence of Cys-Cu NC and H_2O_2, the rate constant (k) and half-life ($t_{1/2}$) for each reaction were determined. The dye concentrations at different time intervals were plotted as a function of time. To elucidate the reaction order, the resulting plots were fitted to appropriate kinetic models, and the corresponding half-lives were calculated.

2.6. Sample preparation for mass spectrometry

For better spectral resolution, the sample obtained after degradation was diluted tenfold (100 μL of the sample diluted to 1 mL with Milli-Q water) before being subjected to mass spectrometric analysis. The control samples containing RhB, MB, and cysteine were also diluted in Milli-Q water to final concentrations of 4.8 mg L^{-1}, 3 mg L^{-1}, and 12.1 mg L^{-1}, respectively, prior to mass spectrometric analysis.

2.7. Sample preparation for NMR spectroscopy

20 mL of the degraded sample, obtained following the procedure described in Section 2.4, was taken in a round-bottom flask, and the solvent was removed using a rotary evaporator. The resulting solid residue was then dissolved in D_2O for ^{1}H NMR analysis. Additionally, ^{1}H NMR spectra of the control samples – RhB, MB and Cys – were recorded by dissolving appropriate amounts of each solid in D_2O to enable comparative analysis.

2.8. Free radical scavenging experiments

To identify the reactive species responsible for dye degradation and to elucidate the underlying mechanism, free radical scavenging experiments were performed. After the sequential addition of Cys-Cu NC, H_2O_2, and the dye, 19.2 μL of TBA and 20 μL of DHBQ were introduced separately into two reaction systems as scavengers for hydroxyl radicals ($^{\bullet}$OH) and superoxide radicals ($^{\bullet}O_2^-$), respectively. The degradation of the dyes was subsequently monitored under identical experimental conditions.

2.9. Scalability and real sample analysis

The scalability of the proposed degradation protocol was evaluated by performing the degradation of RhB and MB at larger reaction volumes while maintaining constant concentrations of Cys-Cu NC, H_2O_2, and the dyes. For this purpose, 25 mL of Cys-Cu NC solution (pH 7) was mixed with 127 μL of H_2O_2 and 333 μL of the respective stock dye solution to achieve a final dye concentration of 20 μM, and the degradation was monitored over time. Similarly, reactions were conducted in 50 mL of Cys-

Cu NC solution containing 255 μL of H_2O_2 and 666 μL of the respective stock dye under identical conditions.

The validity of the developed method was further examined using real water samples. In this case, 200 μL of polluted pond water was added to 1.8 mL of Cys-Cu NC solution, and the degradation of RhB and MB was analyzed following the same experimental protocol. The results obtained from the pond water samples were compared with those using Milli-Q water to assess the performance of the system under real environmental conditions.

2.10. Statistical analysis

The errors reported in the manuscript represent the standard error of the mean (SEM) calculated from at least three independent measurements, unless otherwise stated.

3. Results and discussion

3.1. Cys-Cu NC-mediated degradation of rhodamine B (RhB) and methylene blue (MB)

In this study, the Cys-Cu NCs-mediated degradation of RhB was first investigated. RhB, a common and toxic environmental pollutant,[24,41] exhibited remarkable stability in aqueous solution (pH 7) under vigorous stirring at 50 °C. Time-dependent absorption measurements showed that the absorption spectrum (λ_{abs}^{max} = 553 nm) of RhB (~20 μM, 9.6 mg L^{-1}) remained essentially unchanged even after 22 hours, demonstrating its remarkable stability (Fig. S1A). Upon the addition of Cys-Cu NCs alone, no appreciable change in the absorption spectra was observed (Fig. S1B). However, the introduction of both Cys-Cu NCs and H_2O_2 led to a rapid decrease in the absorbance under neutral conditions, suggesting efficient dye degradation through a synergistic effect between H_2O_2 and the nanoclusters (Fig. 1A and B). Within 90 minutes, the reaction mixture gradually changed colour from pink to colourless, signifying the complete degradation of RhB (Fig. 1C). Quantitatively, the dye concentration decreased from 20 μM to 0.63 μM, corresponding to ~97% degradation (Fig. 1A and B).

Control experiments confirmed that the Cys-Cu NC + H_2O_2 system exhibited markedly superior degradation efficiency than either component alone. While H_2O_2 alone caused a minor decrease (~20% within 90 minutes), the combined system achieved near-complete degradation (Fig. S2 and 1B). Importantly, no shift in the absorption maximum was detected throughout the reaction (Fig. 1A), indicating the absence of intermediate species or side-product formation. Fluorescence emission spectra of the reaction mixture further validated the degradation process. RhB displayed a characteristic emission peak at 586 nm upon excitation at 553 nm. After 90 minutes of reaction, the photoluminescence (PL) intensity at 586 nm was completely quenched, further confirming the complete degradation of RhB (Fig. S3).

The degradation studies mediated by Cys-Cu NCs were further extended to other organic dyes to assess whether the process was specific to RhB or applicable to a broader range of pollutants. MB, a widely used dye in the textile industry and a known environmental contaminant due to its toxicity and persistence,[47,48] was chosen as an additional model compound.

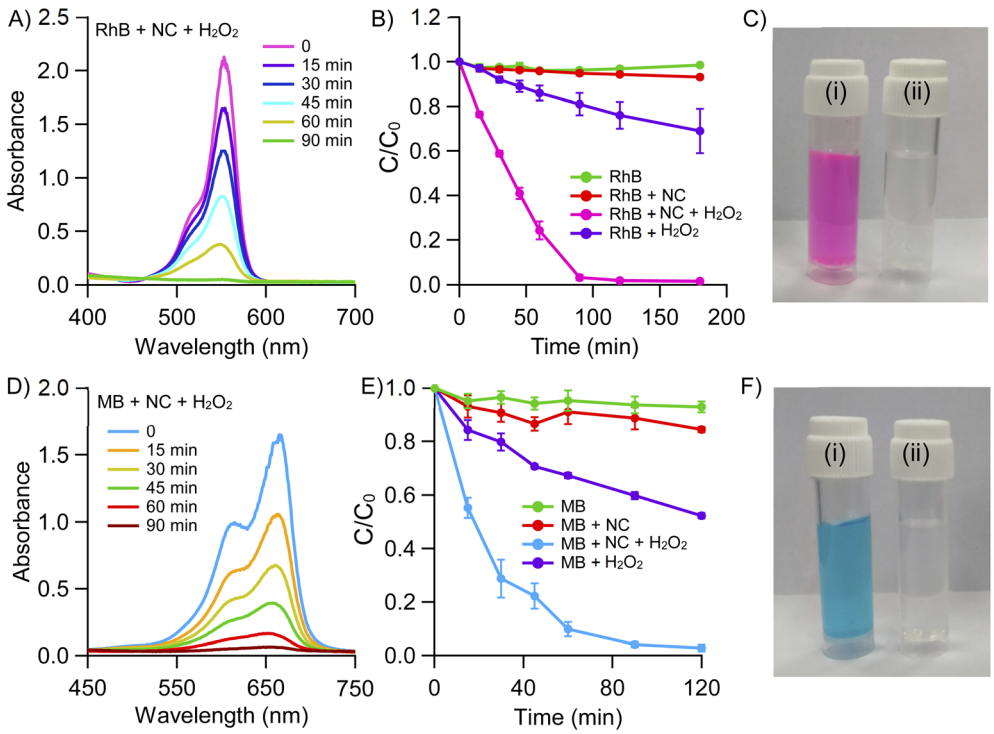

Fig. 1 Cys-Cu NC-mediated degradation of (A–C) RhB and (D–F) MB: time-dependent absorption spectra of (A) RhB and (D) MB with Cys-Cu NC + H_2O_2. Degradation profiles (C/C_0 *vs.* time) of (B) RhB and (E) MB with Cys-Cu NC + H_2O_2 and with different controls. Solution colour changes of (C) RhB and (F) MB (i) before and (ii) after degradation.

Similar to RhB, MB (~20 μM, 6.4 mg L^{-1}) exhibited high stability under neutral pH (7.0) and vigorous stirring at 50 °C, showing negligible changes in its absorbance profile (Fig. S4). The degradation of MB was monitored following the same procedure used for RhB, in the presence of Cys-Cu NCs and H_2O_2. A gradual decrease in the absorbance of MB ($\lambda_{abs}^{max} = 665$ nm) was observed over time, accompanied by a distinct colour change from blue to colourless (Fig. 1D–F). Within 60 minutes, more than 90% degradation of MB was achieved—slightly faster than that observed for RhB (76%)—and after 90 minutes, the dye concentration decreased from 20 μM to ~0.6 μM, corresponding to a degradation efficiency of ~97% (Fig. 1D and E).

Control experiments were conducted in the absence and presence of individual components (H_2O_2 or Cys-Cu NCs) to evaluate their respective contributions. The results revealed a trend consistent with that observed for RhB: Cys-Cu NCs alone showed

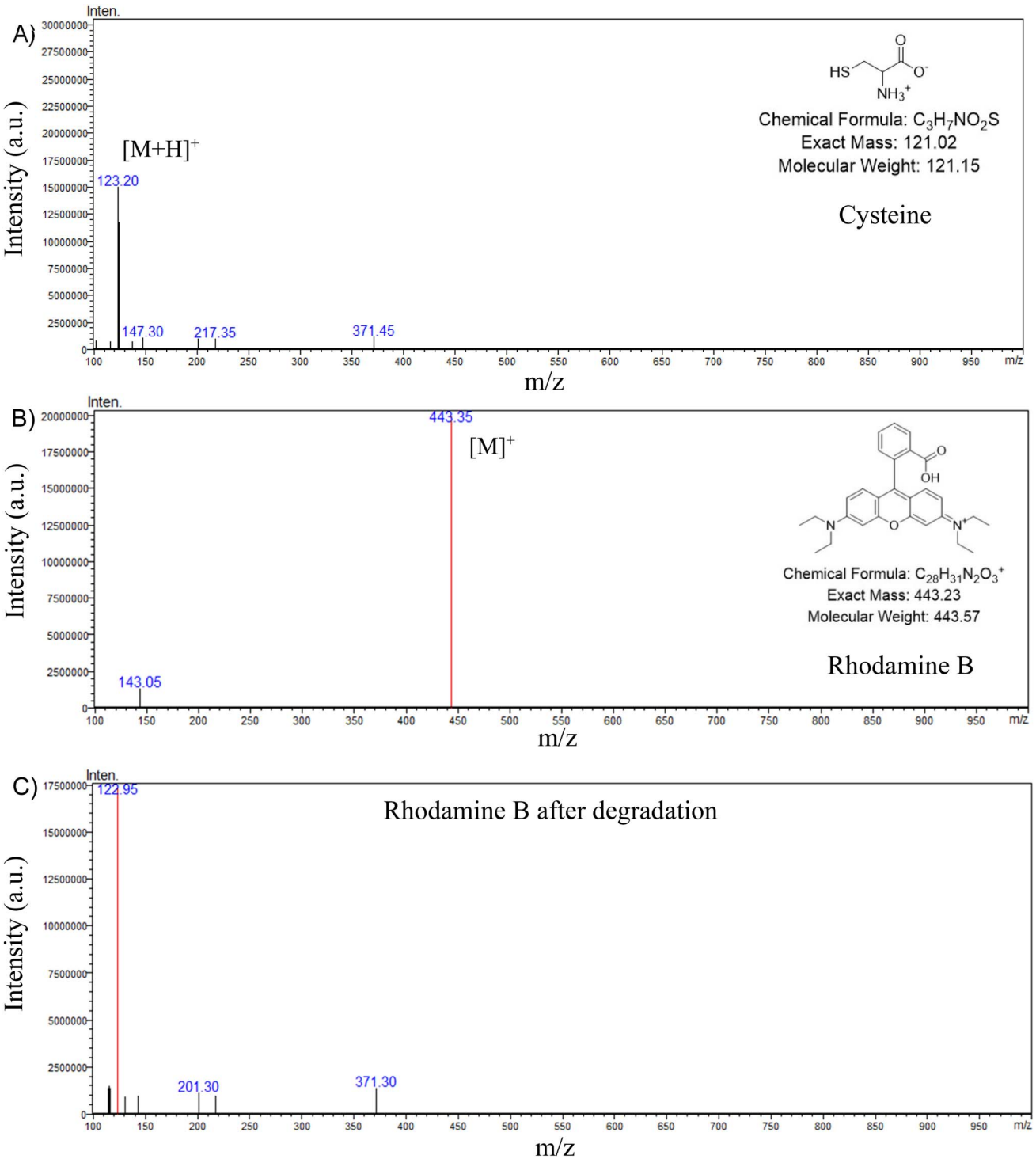

Fig. 2 LC-MC Mass spectra of (A) pure Cys, (B) pure RhB, (C) RhB after degradation in presence of Cys-Cu NC and H_2O_2.

negligible activity, while H_2O_2 alone induced only minor degradation, significantly lower than the combined Cys-Cu NC + H_2O_2 system (Fig. 1E). Overall, the synergistic action of Cys-Cu NCs and H_2O_2 proved to be a highly effective and general strategy for the degradation of both RhB and MB, highlighting its potential applicability toward other organic dyes as well. The observed degradation time-scale and percentage were better or comparable with other photocatalysts or degradation methods for these two dyes (Table S1). Further investigation of the mechanistic and kinetic aspects of this degradation process could provide valuable insights into the underlying reaction pathways.

3.2. Verification of degradation end products

One of the major challenges in dye degradation processes—and a key advantage of our system—is achieving complete mineralization of dyes without generating any secondary toxic by-products. To verify this, the possible end products after degradation were examined and compared with pure RhB/MB and the amino acid scaffold, Cys, using different analytical techniques such as LC-MS, ^{1}H-NMR, and ion chromatography.

The LC-MS spectra of Cys and RhB (Fig. 2A and B) displayed characteristic peaks at *m/z* 123.2 ($[M + H]^+$ for Cys)[59] and *m/z* 443.35 ($[M]^+$ for RhB),[60,61] respectively. After 90 minutes of degradation, the LC-MS spectrum of the reaction mixture (Fig. 2C) showed a complete disappearance of the RhB peak at *m/z* 443.35, confirming full degradation of the dye. A residual peak at *m/z* 122.95 corresponded to undegraded Cys, while the absence of any additional characteristic peaks indicated complete mineralization of RhB, leaving Cys as the only detectable species. A similar observation was made for MB. The molecular ion peak of MB at *m/z* 284.3,[62] was entirely absent in the degraded sample, and only a prominent peak at *m/z* 123.2, corresponding to Cys, was detected (Fig. S5). This confirmed that MB also underwent complete mineralization with no detectable intermediates or secondary products.

To further validate the complete breakdown of the dyes, the degraded samples were analyzed by ^{1}H NMR spectroscopy in D_2O, using pure dyes and Cys as controls (Fig. 3). The spectrum of Cys exhibited a characteristic signal at 3.9 ppm corresponding to the α-proton, along with multiplet peaks between 3.09–2.97 ppm attributed to β-protons.[63] Pure RhB and MB, on the other hand, displayed distinct aromatic proton peaks in the range of 8.0–6.5 ppm (Fig. 3).[64,65] Additionally, RhB showed diethyl proton signals at 3.4 and 1.13 ppm, whereas MB exhibited a methyl proton signal at 3.16 ppm.[64,65] In the spectra of the degraded samples, all characteristic signals corresponding to aromatic, ethyl, and methyl protons were completely absent (Fig. 3), confirming the total decomposition of RhB and MB without the formation of any detectable organic intermediates. Interestingly, the disappearance of Cys-related multiplets in the 3.09–2.97 ppm region indicates its degradation during the process, with only a small residual peak at 3.9 ppm corresponding to a trace amount of the unreacted Cys (Fig. 3).

Previous studies report that during complete mineralization of RhB and MB, in addition to CO_2 and H_2O, RhB generates NO_3^- and NH_4^+, whereas MB produces NO_3^- and SO_4^{2-}.[66,67] To

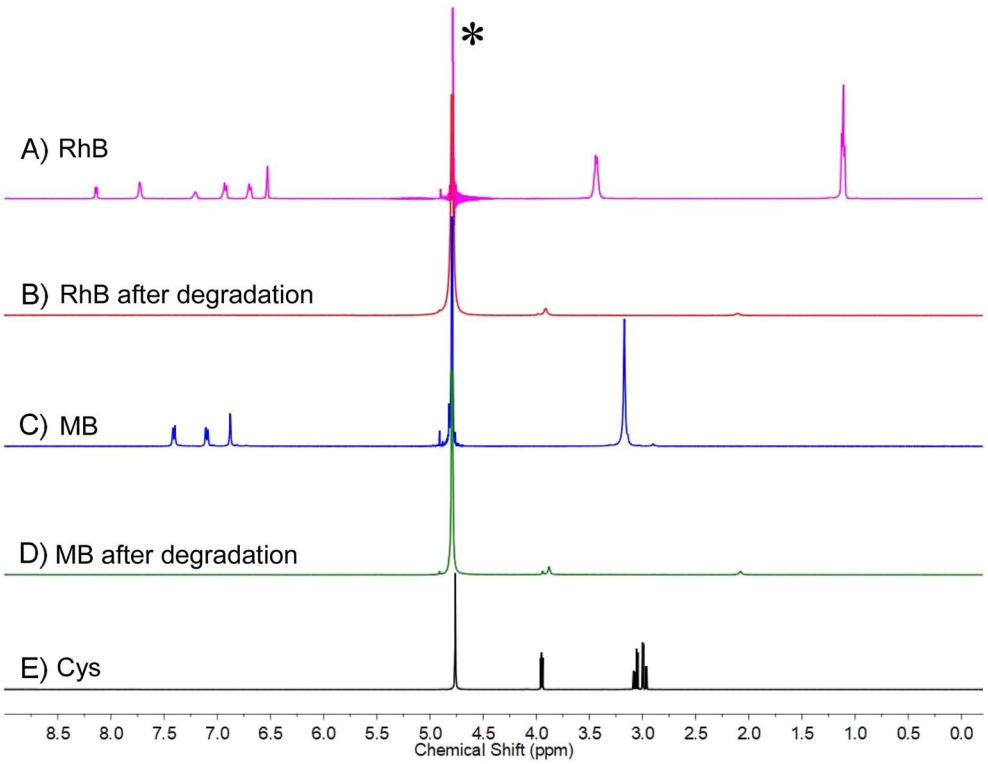

Fig. 3 ^{1}H-NMR spectra of (A) pure RhB (pink), (B) RhB after degradation in the presence of Cys-Cu NC and H_2O_2 (red), (C) pure MB (blue), (D) MB after degradation in the presence of Cys-Cu NC and H_2O_2 (green), and (E) pure Cys (black). The strong solvent peak of D_2O observed at 4.79 ppm is denoted by an asterisk (*).

confirm the formation of these anions, ion chromatography was performed on the post-degradation samples of RhB and MB. The analysis confirmed the presence of NO_3^- and SO_4^{2-}, along with Cl^- (Fig. S6). The SO_4^{2-} detected in the RhB-degraded sample likely originated from Cys degradation, while the Cl^- ions in both samples can be attributed to the HCl used for pH adjustment. These observations collectively confirm that the developed system enables complete mineralization of the dyes into non-toxic, non-hydrocarbon species.

3.3. Mechanism of dye degradation

The copper core in Cys-Cu NCs predominantly consists of Cu^0 with a trace amount of Cu^+, as demonstrated by XPS analysis in earlier studies.[56] Due to its propensity for oxidation, Cu^0/Cu^+ can readily convert to Cu^{2+} in the presence of H_2O_2, generating ROS such as hydroxyl radicals ($^{\bullet}OH$). To elucidate the fate of copper and the role of the metal core in facilitating dye degradation, XPS analysis was performed on the post-reaction sample. The spectrum exhibited two additional satellite peaks, in addition to the main Cu $2p_{3/2}$ (932.1 eV) and Cu $2p_{1/2}$ (952.0 eV) peaks corresponding to Cu^0/Cu^+. These satellites, located around 942.0 eV and 962.0 eV, respectively, confirm the formation of Cu^{2+} species in the degraded sample (Fig. 4A).[68–70] The pronounced oxidative response of the nanocluster toward H_2O_2 was further corroborated by the quenching of its photoluminescence (PL) intensity (Fig. S7).[56] Therefore, the degradation of dyes can be attributed to redox reactions between the copper core of the nanocluster and H_2O_2, leading to the generation of ROS, which are responsible for efficient dye degradation.

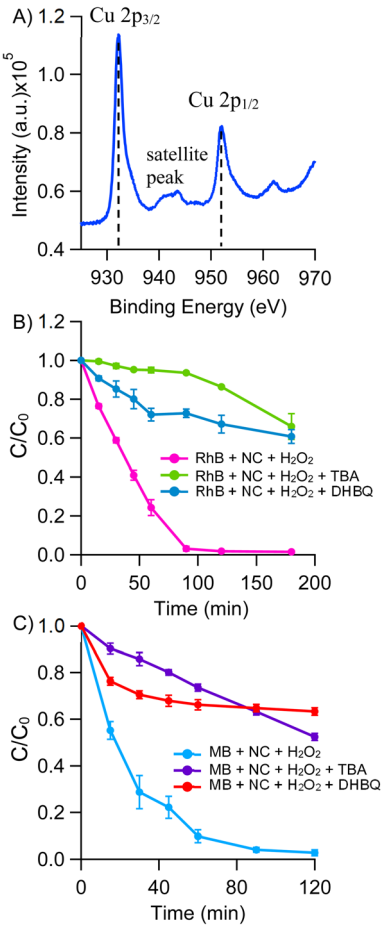

Fig. 4 (A) XPS spectrum of the sample obtained after RhB degradation using Cys-Cu NC and H_2O_2. Degradation profiles (C/C_0 *vs.* time) of (B) RhB and (C) MB in the absence and presence of free radical scavengers TBA and DHBQ.

To assess the role of the redox properties of the metal core, the degradation of RhB was further evaluated using an additional amino acid-scaffolded copper nanoclusters, namely Trp-Cu NCs. Among the two nanoclusters, Cys-Cu NCs demonstrated higher degradation efficiency (Fig. S8). Notably, Cys or Trp alone, either in the absence or presence of H_2O_2, did not exhibit any dye degradation (Fig. S9), confirming that the observed activity can be ascribed to the copper core. Although the presence of copper in Trp-Cu NCs contributed to effective dye degradation, the overall rate was slightly lower, with approximately 70% degradation of RhB achieved within 90 minutes. This difference is likely attributable to the nature of the coordinating scaffold, which does not directly participate in dye degradation but modulates the stability and redox accessibility of the metal core. Consequently, Trp-Cu NCs exhibit greater resistance to oxidation in the presence of H_2O_2 than Cys-Cu NCs, resulting in a slightly reduced degradation rate.[27,56]

To identify the primary reactive species responsible for dye degradation, control experiments were performed using specific radical scavengers—*tert*-butyl alcohol (TBA) for hydroxyl radicals ($^{\bullet}OH$) and 2,5-dihydroxy-*p*-benzoquinone (DHBQ) for superoxide radicals ($^{\bullet}O_2^-$).[70,71] In the presence of either scavenger, a noticeable reduction in the slope of the C/C_0 *versus* time plots was observed, indicating a slower degradation rate of both RhB and MB (Fig. 4B and C). For RhB, the degradation efficiency after 90 minutes dropped dramatically from ~97% to ~6% and ~27% upon addition of TBA and DHBQ, respectively. A similar trend was observed for MB, with degradation efficiencies decreasing to ~36% (TBA) and ~35% (DHBQ) after 90 minutes. These results confirm the crucial roles of $^{\bullet}OH$ and $^{\bullet}O_2^-$ radicals in the degradation process. The interaction of the copper core of the nanocluster with H_2O_2, in the presence of visible light, generates $^{\bullet}OH$ and $^{\bullet}O_2^-$ radicals, which facilitate the stepwise degradation of the dyes into low-molecular-weight, non-toxic products. Based on the XPS analysis, scavenger experiments, and previously reported studies,[25,67,72–74] the degradation mechanism for both organic dyes can be proposed as follows:

$$Cu^0 \rightarrow Cu^{2+} + 2e^-$$

$$Cu^+ \rightarrow Cu^{2+} + e^-$$

$$H_2O_2 + e^- \rightarrow OH^- + {}^{\bullet}OH$$

$$O_2 + e^- \rightarrow {}^{\bullet}O_2^-$$

$$\text{RhB/MB} + {}^{\bullet}OH/{}^{\bullet}O_2^- \rightarrow CO_2 + H_2O + \text{inorganic anions } (NO_3^-, SO_4^{2-})$$

3.4. Kinetics of dye degradation

To investigate the degradation kinetics of RhB and MB in the presence of Cys-Cu NCs and H_2O_2, dye concentrations at different time intervals were calculated from their absorbance maxima and plotted against time, enabling determination of the corresponding kinetic order, rate constants (k) and half-lives ($t_{1/2}$). For RhB, a linear decrease in concentration with time was observed, indicating unusual zero-order kinetics (Fig. 5A). The rate constant, determined from the slope, was 0.25 μM min^{-1}, corresponding to a half-life of 40 minutes. In contrast, MB exhibited an exponential decay in concentration, consistent with first-order kinetics (Fig. 5B), as commonly reported in earlier studies.[75] The rate constant was calculated as 0.035 min^{-1}, with a corresponding half-life of 20 minutes, indicating a faster degradation than RhB. Thus, although both RhB and MB undergo efficient degradation under identical conditions in the presence of Cys-Cu NCs and H_2O_2, the kinetic analysis reveals that they degrade at different rates and follow distinct kinetic pathways.

3.5. Scalability and real-world applicability

Degradation studies were carried out at varying dye concentrations to evaluate the efficiency and robustness of the Cys-Cu NC–H_2O_2 system under different dosages. Under identical conditions and fixed Cys-Cu NC concentration, the initial concentrations of RhB and MB were varied from 5 to 100 μM (2.4 to 48 mg L^{-1}), and the degradation efficiency was monitored over time. For RhB, approximately 93% degradation was achieved within 45 minutes at 5 μM, while nearly complete degradation (>97%) required 60, 90, 120, and 240 minutes for 10, 20, 50, and 100 μM RhB, respectively (Fig. S10). A similar concentration-dependent trend was observed for MB. These results indicate that the degradation efficiency of the system remains high even at elevated dye concentrations.

To assess the scalability of the process, degradation experiments were performed at larger reaction volumes (25 mL and 50 mL) containing 20 μM of each dye, while maintaining the same dye: Cys-Cu NC–H_2O_2 ratio as in the smaller-scale experiments. At a 25 mL scale, using the same concentrations of Cys-Cu NC and H_2O_2, degradation efficiencies of 99.6% (RhB) and 98.9% (MB) were achieved within 180 minutes. When the reaction volume was increased to 50 mL, efficiencies of 98.9% for RhB and 99.7% for MB were obtained within 300 minutes. These results demonstrate that the system maintains comparable degradation performance upon scale-up, with only a modest increase in reaction time. The process can be further accelerated by proportionally increasing the Cys-Cu NC dosage, highlighting its potential for larger-scale applications.

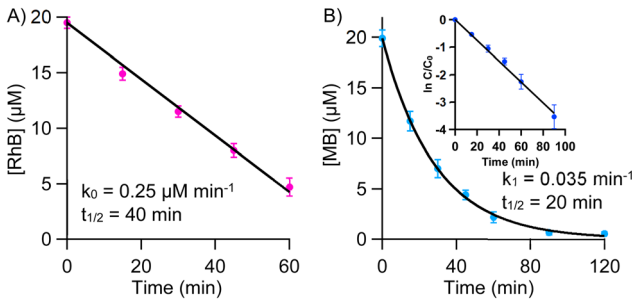

Fig. 5 Kinetic study of degradation: concentration *vs.* time plot for (A) RhB (pink) shows a linear fit (black), indicating zero-order kinetics, while (B) MB (sky blue) follows an exponential fit (black), characteristic of first-order kinetics. Inset of B shows the corresponding ln(C/C_0) *vs.* time plot (blue) with linear fits (black).

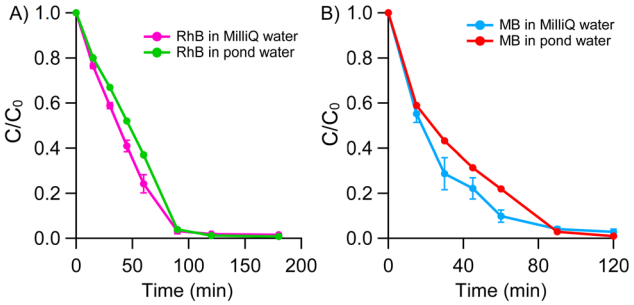

Fig. 6 Degradation profiles (C/C_0 *vs.* time) of (A) RhB and (B) MB carried out in Milli-Q water and pond water.

The degradation performance was further validated using real water samples collected from a polluted pond. Although the absorption spectrum of the pond water showed noticeable absorbance in the UV region, no measurable absorbance was observed at 553 nm or 665 nm (Fig. S11). This confirms that the inherent contaminants did not contribute to the signals at these wavelengths. The pond water was spiked with 20 μM RhB or MB, and degradation studies were conducted under identical conditions. After 90 minutes, degradation efficiencies of 96% for RhB and 97% for MB were achieved (Fig. 6), closely matching those obtained in Milli-Q water. This demonstrates that the presence of impurities or competing species in natural water had minimal impact on the degradation performance, confirming the practical applicability of the Cys-Cu NC–H_2O_2 system for real-world wastewater treatment. Overall, these results underscore the robustness and scalability of the Cys-Cu NC–H_2O_2 system, demonstrating its strong potential for practical wastewater treatment applications.

4. Conclusions

This study demonstrated the potential of Cys-Cu NCs as an efficient, simple and environmentally benign system for the degradation of toxic organic dyes. The synergistic Cys-Cu NC–H_2O_2 system effectively degraded both RhB and MB under aqueous and neutral conditions without the need for external irradiation or harsh reagents. UV-visible absorption and PL spectra recorded during the degradation process revealed a progressive decrease in both absorbance and PL intensity over time, achieving approximately 97% degradation of both dyes within 90 minutes. Complementary LC-MS, ^{1}H NMR, and ion chromatography studies verified that the dyes were fully mineralized into non-toxic end products. Mechanistic investigations established $^{\bullet}OH$ and $^{\bullet}O_2^-$ radicals as the key reactive oxygen species driving the degradation process. The observed

superior activity of Cys-Cu NCs, as compared to other nanoclusters, underscores the crucial role of copper's redox behaviour in driving ROS formation and subsequent dye degradation. Kinetic studies revealed distinct reaction orders with RhB following zero-order kinetics and MB following first-order kinetics. Importantly, the process maintained its efficiency in real water samples and at larger reaction volumes, demonstrating strong scalability and environmental relevance. Overall, this work not only provides mechanistic insights into nanocluster-mediated advanced oxidation processes but also presents a sustainable and practical approach for wastewater remediation using amino acid–stabilized metal nanoclusters, while minimizing the production of hazardous byproducts. The simplicity, high efficiency, and green nature of the method make it a promising candidate for future large-scale water treatment applications.

Author contributions

Aarya: investigation, validation, data curation, formal analysis, methodology, writing – original draft. Kavya P.: investigation, formal analysis. Chanchal N. S.: investigation. Devika V.: investigation. Athira Sathyan: investigation. Supratik Sen Mojumdar: conceptualization, funding acquisition, methodology, supervision, formal analysis, writing – original draft.

Conflicts of interest

There are no conflicts of interest to declare.

Data availability

Data are available from the authors upon reasonable request.

Supplementary information (SI) is available. See DOI: https://doi.org/10.1039/d5ra08780e.

Acknowledgements

Aarya & K. P. thank UGC, Government of India, for providing fellowships. C. N. S., D. V. and A. S. are grateful to IIT Palakkad for their fellowships. S. S. M. thanks ANRF, Government of India (Project No. CRG/2022/007366), and IIT Palakkad for financial assistance. S. S. M. thanks the central instrumentation facility (CIF) at IIT Palakkad for LC-MS characterization facility, the Advanced Material Research Centre (AMRC) at IIT Mandi for XPS analysis, NIT Calicut for ^{1}H-NMR analysis and DST SAIF Cochin for ion chromatography analysis. The authors thank Ms Kashish Jain for her valuable insights and assistance with the experiments.

References

1 K. Saravanakumar, S. De Silva, S. S. Santosh, A. Sathiyaseelan, A. Ganeshalingam, M. Jamla, A. Sankaranarayanan, V. P. Veeraraghavan, D. MubarakAli, J. Lee, G. Thiripuranathar and M.-H. Wang, *Chemosphere*, 2022, **307**, 135593.
2 M. Date and D. Jaspal, *Ind. Eng. Chem. Res.*, 2023, **62**, 20492–20505.
3 S. Dutta, B. Gupta, S. Kumar Srivastava and A. Kumar Gupta, *Mater. Adv.*, 2021, **2**, 4497–4531.
4 K. F. Kayani, S. J. Mohammed, M. S. Mustafa and S. B. Aziz, *Mater. Adv.*, 2025, **6**, 5391–5409.
5 S. Kundu, T. Sarkar, A. A. Al-Ahmadi, E. Ali and A. Bhattacharjee, *RSC Adv.*, 2024, **14**, 28944–28955.
6 S. Khan, T. Noor, N. Iqbal and L. Yaqoob, *ACS Omega*, 2024, **9**, 21751–21767.
7 J. Sharma, S. Sharma and V. Soni, *Reg. Stud. Mar. Sci.*, 2021, **45**, 101802.
8 K.-T. Chung, *J. Environ. Sci. Health, Part C*, 2016, **34**, 233–261.
9 Z. Wang, M. Gao, X. Li, J. Ning, Z. Zhou and G. Li, *Mater. Sci. Eng. C*, 2020, **108**, 110196.
10 Saruchi, V. Kumar, B. S. Kaith and R. Jindal, *Ind. Eng. Chem. Res.*, 2016, **55**, 10492–10499.
11 G. Zhang, S. Wang, S. Zhao, L. Fu, G. Chen and F. Yang, *Appl. Catal., B*, 2011, **106**, 370–378.
12 S. Kim, M. Yu and Y. Yoon, *ACS Appl. Mater. Interfaces*, 2020, **12**, 16557–16565.
13 F. Banat, S. Al-Asheh and M. Qtaishat, *Desalination*, 2005, **174**, 87–96.
14 M. C. García, M. Mora, D. Esquivel, J. E. Foster, A. Rodero, C. Jiménez-Sanchidrián and F. J. Romero-Salguero, *Chemosphere*, 2017, **180**, 239–246.
15 Y.-Y. Lau, Y.-S. Wong, T.-T. Teng, N. Morad, M. Rafatullah and S.-A. Ong, *RSC Adv.*, 2015, **5**, 34206–34215.
16 Md. Islam, J. Akter, I. Lee, S. Shrestha, A. Pandey, N. Gyawali, Md. Hossain, Md. Hanif, S. Jang and J. Hahn, *Nanomaterials*, 2022, **12**, 3959.
17 M. Ahtasham Iqbal, S. Akram, S. Khalid, B. Lal, S. U. Hassan, R. Ashraf, G. Kezembayeva, M. Mushtaq, N. Chinibayeva and A. Hosseini-Bandegharaei, *Environ. Res.*, 2024, **253**, 118947.
18 A. Haleem, M. Ullah, S. U. Rehman, A. Shah, M. Farooq, T. Saeed, I. Ullah and H. Li, *Water*, 2024, **16**, 1588.
19 P. Sharma, M. Ganguly and M. Sahu, *RSC Adv.*, 2024, **14**, 11411–11428.
20 M. S. Mathew, G. Krishnan, A. A. Mathews, K. Sunil, L. Mathew, R. Antoine and S. Thomas, *Nanomaterials*, 2023, **13**, 1874.
21 H. Zhu, N. Goswami, Q. Yao, T. Chen, Y. Liu, Q. Xu, D. Chen, J. Lu and J. Xie, *J. Mater. Chem. A*, 2018, **6**, 1102–1108.
22 A. Okram, M. Singh and A. K. Singh, *ChemistrySelect*, 2025, **10**, e01804.
23 T. Goswami, M. Singh, K. M. Reddy and A. K. Mishra, *ChemistrySelect*, 2018, **3**, 10892–10899.
24 T. L. Yusuf, B. O. Orimolade, D. Masekela, B. Mamba and N. Mabuba, *RSC Adv.*, 2022, **12**, 26176–26191.
25 C. Xie, X. Wen, C. Xiao, S. Wei, X. Wu, S. Liu and J. Cao, *Water, Air, Soil Pollut.*, 2020, **231**, 280.
26 R. Ghosh, A. K. Sahoo, S. S. Ghosh, A. Paul and A. Chattopadhyay, *ACS Appl. Mater. Interfaces*, 2014, **6**, 3822–3828.
27 Aarya, T. Thomas, B. R. Sarangi and S. Sen Mojumdar, *ACS Omega*, 2023, **8**, 14630–14640.
28 H. Li, H. Li and A. Wan, *Analyst*, 2020, **145**, 348–363.

29 A. Sebastian, Aarya, B. R. Sarangi and S. Sen Mojumdar, *J. Photochem. Photobiol., A*, 2023, **436**, 114378.
30 A. A. Buglak and M. T. Nguyen, *Biophys. Rev.*, 2024, **16**, 441–477.
31 Y. Chen, M. L. Phipps, J. H. Werner, S. Chakraborty and J. S. Martinez, *Acc. Chem. Res.*, 2018, **51**, 2756–2763.
32 B. Casteleiro, F. Da Cruz-Boisson, P. Alcouffe, S. N. Pinto, J. M. Gaspar Martinho, M.-T. Charreyre, J. P. S. Farinha and A. Favier, *ACS Appl. Nano Mater.*, 2023, **6**, 11689–11698.
33 W. Cui, L. Wang, G. Xiang, L. Zhou, X. An and D. Cao, *Sens. Actuators, B*, 2015, **207**, 281–290.
34 A. Raza, S. Javed, M. Z. Qureshi, M. U. Khan and M. S. Khan, *Appl. Nanosci.*, 2017, **7**, 429–437.
35 K. Anusuyadevi, S. P. Wu and S. Velmathi, *J. Photochem. Photobiol., A*, 2021, **421**, 113526.
36 Z. Cai, R. Zhu, S. Chen, L. Wu, K. Qi and C. Zhang, *ChemistrySelect*, 2020, **5**, 3682–3687.
37 Aarya, A. Sebastian, K. P, I. Bhattacharjee, A. S. Shekhawat, B. R. Sarangi and S. Sen Mojumdar, *Mater. Adv.*, 2025, **6**, 4714–4724.
38 K. P. Aarya, A. Sebastian and S. Sen Mojumdar, *Sens. Actuators, B*, 2024, **401**, 134923.
39 S. Ullah, Q. Li, R. Ullah, S. Anwar, M. F. Hameed and M. Zhu, *Nanoscale Adv.*, 2023, **5**, 3326–3335.
40 H. Battula, S. Bommi, Y. Bobde, T. Patel, B. Ghosh and S. Jayanty, *J. Photochem. Photobiol.*, 2021, **6**, 100026.
41 N. Mzimela, S. Tichapondwa and E. Chirwa, *RSC Adv.*, 2022, **12**, 34652–34659.
42 L. Peng, P. Qin, M. Lei, Q. Zeng, H. Song, J. Yang, J. Shao, B. Liao and J. Gu, *J. Hazard. Mater.*, 2012, **209–210**, 193–198.
43 S. Sudarshan, V. S. Bharti, S. Harikrishnan, S. P. Shukla and G. RathiBhuvaneswari, *Arch. Microbiol.*, 2022, **204**, 658.
44 P. S. Priya, P. Pratiksha Nandhini, S. Vaishnavi, V. Pavithra, M. H. Almutairi, B. O. Almutairi, S. Arokiyaraj, R. Pachaiappan and J. Arockiaraj, *Comp. Biochem. Physiol., Part C: Toxicol. Pharmacol.*, 2024, **280**, 109898.
45 C. Tatebe, X. Zhong, T. Ohtsuki, H. Kubota, K. Sato and H. Akiyama, *Food Sci. Nutr.*, 2014, **2**, 547–556.
46 *Some Chemicals that Cause Tumours of the Kidney or Urinary Bladder in Rodents and Some Other Substances*, ed. Centre international de recherche sur le cancer, IARC, Lyon, 1999.
47 M. Contreras, C. D. Grande-Tovar, W. Vallejo and C. Chaves-López, *Water*, 2019, **11**, 282.
48 P. O. Oladoye, T. O. Ajiboye, E. O. Omotola and O. J. Oyewola, *Results Eng.*, 2022, **16**, 100678.
49 D. Bosoy, J. Axelband, R. Pursell, J. Lukaszczyk and S. Stawicki, *Int. J. Acad. Med.*, 2017, **3**, 101.
50 K. Allegaert, M. Miserez, T. Lerut, G. Naulaers, C. Vanhole and H. Devlieger, *J. Pediatr. Surg.*, 2004, **39**, E35–E37.
51 V. K. Gupta, D. Pathania, S. Agarwal and S. Sharma, *J. Mol. Liq.*, 2012, **174**, 86–94.
52 A. Rovisco, R. Branquinho, J. Deuermeier, T. Freire, E. Fortunato, R. Martins and P. Barquinha, *ACS Appl. Nano Mater.*, 2021, **4**, 1149–1161.
53 I. Khan, K. Saeed, I. Zekker, B. Zhang, A. H. Hendi, A. Ahmad, S. Ahmad, N. Zada, H. Ahmad, L. A. Shah, T. Shah and I. Khan, *Water*, 2022, **14**, 242.
54 P. K. Gillman, *Anaesthesia*, 2006, **61**, 1013–1014.
55 A. Krishna Moorthy, B. Govindarajan Rathi, S. P. Shukla, K. Kumar and V. Shree Bharti, *Environ. Toxicol. Pharmacol.*, 2021, **82**, 103552.
56 K. P, A. Sebastian, Aarya, A. Sathyan and S. Sen Mojumdar, *Chem.–Asian J.*, 2025, **20**, e00169.
57 N. O. Mchedlov-Petrosyan and Yu. V. Kholin, *Russ. J. Appl. Chem.*, 2004, **77**, 414–422.
58 J.-C. Bollinger, E. C. Lima, L. Mouni, S. Salvestrini and H. N. Tran, *Environ. Chem. Lett.*, 2025, **23**, 1403–1424.
59 D. Trivedi, M. K. Trivedi, A. Branton and S. Jana, *JOJMS*, 2021, **6**, 59–63.
60 B. R. V. Ferreira, D. N. Correa, M. N. Eberlin and P. H. Vendramini, *J. Braz. Chem. Soc.*, 2017, **28**, 136–142.
61 F. Sabatini, R. Giugliano and I. Degano, *Microchem. J.*, 2018, **140**, 114–122.
62 O. M. A. Halim, N. H. Mustapha, S. N. Mohd Fudzi, R. Azhar, N. I. N. Zanal, N. F. Nazua, A. H. Nordin, M. S. Mohd Azami, M. A. Mohd Ishak, W. I. N. Wan Ismail and Z. Ahmad, *Results Surf. Interfaces*, 2025, **18**, 100408.
63 R. J. Dougherty, J. Singh and V. V. Krishnan, *J. Mol. Struct.*, 2017, **1131**, 196–200.
64 G. S. G. De Carvalho, M. M. De Siqueira, M. P. Do Nascimento, M. A. L. De Oliveira and G. W. Amarante, *Heliyon*, 2020, **6**, e04128.
65 M. Pandurangappa and K. S. Kumar, *Anal. Methods*, 2011, **3**, 715.
66 S. Wang, Y. Jia, L. Song and H. Zhang, *ACS Omega*, 2018, **3**, 18456–18465.
67 J. Zhang, K. Lei, J. Cheng, L. Luo, X. Liu and J. Li, *J. Alloys Compd.*, 2023, **958**, 170494.
68 M. C. Biesinger, *Surf. Interface Anal.*, 2017, **49**, 1325–1334.
69 S. Poulston, P. M. Parlett, P. Stone and M. Bowker, *Surf. Interface Anal.*, 1996, **24**, 811–820.
70 Y. Guo, C. Zhou, L. Fang, Z. Liu, W. Li and M. Yang, *ACS Omega*, 2021, **6**, 8119–8130.
71 J. T. Schneider, D. S. Firak, R. R. Ribeiro and P. Peralta-Zamora, *Phys. Chem. Chem. Phys.*, 2020, **22**, 15723–15733.
72 Y. Wang, Y. Tan, Y. Ding, L. Fu and W. Qing, *Colloids Surf., A*, 2022, **654**, 130072.
73 S. Ullah, Q. Li, R. Ullah, S. Anwar, M. F. Hameed and M. Zhu, *Nanoscale Adv.*, 2023, **5**, 3326–3335.
74 J. Li, P. Guo, E. Li, C. Zhao, X. Yan and P. Xu, *J. Alloys Compd.*, 2025, **1036**, 181860.
75 I. Raheb and M. S. Manlla, *Heliyon*, 2021, **7**, e07427.